JOURNAL OF THERMOPHYSICS AND HEAT TRANSFER
Vol. 23, No. 2, April–June 2009

Thermal Characterization of a Copper Microchannel Heat Sink for Power Electronics Cooling

Randeep Singh* and Aliakbar Akbarzadeh
RMIT University, Bundoora, Victoria 3083, Australia
and
Masataka Mochizuki, Thang Nguyen, and Tien Nguyen
Fujikura, Ltd., Tokyo 135-8512, Japan

DOI: 10.2514/1.40033

An investigative prototype of a single-phase cooling system based on the microchannel heat sink with water as the heat transfer medium was developed to study the fluid flow and forced-convection heat transfer characteristics for the cooling of electronics microprocessors with extremely high heat fluxes. The microchannel heat sink was made from copper with a high fin aspect ratio of 17.5. In the experiment, pressure losses through the heat sink and thermal characteristics of the cooling section under different heat fluxes (25 to 200 W from 7×7 mm^2 and 11×13 mm^2 heat sources) and coolant flow rates (1.7 to 15 cm^3/s) were studied. Under similar test conditions, minimum cold-plate thermal resistances R_{cp} of 0.11 and 0.33°C/W were achieved with 11×13 mm^2 and 7×7 mm^2 sources, respectively. Heat fluxes of up to 4.1 MW/m^2 were effectively dissipated while maintaining a junction temperature below 100°C. With a 15 cm^3/s ($Re = 150$) coolant flow rate, maximum values of 5334 W/m$^2 \cdot$ K for the convection heat transfer coefficient and 3.4 for the Nusselt number were achieved with a 3.3 kPa coolant pressure drop through the system. As an outcome of the present investigation, the copper water-based microchannel heat sink has proved to be a reliable cooling solution for high-end microprocessors.

Nomenclature

A	=	area, m^2
D	=	diameter, m
d	=	depth, m
f	=	Darcy friction factor
h	=	heat transfer coefficient, W/m$^2 \cdot$ K
$\bar{h}$	=	average heat transfer coefficient, W/m$^2 \cdot$ K
I	=	current, A
k	=	thermal conductivity, W/m $\cdot$ K
l	=	length, m
m	=	parameter defined by Eq. (8)
N	=	number of fins
Nu	=	Nusselt number
P	=	perimeter, m
$Q^{\bullet}$	=	heat load, W
R	=	thermal resistance, °C/W, K/W
Re	=	Reynolds number
T	=	temperature, °C, K
t	=	thickness, m
U	=	flow velocity, m/s
V	=	voltage, V
α	=	aspect ratio
ΔP	=	pressure drop, Pa
η	=	efficiency, %
ρ	=	density, kg/m^3

Subscripts

a	=	applied
az	=	active zone
b	=	base
c	=	convection
ch	=	channel
cp	=	cold plate
ct	=	contact
es	=	external spreading
ew	=	external wall
f	=	fin
fc	=	fin cross section
fi	=	fluid inlet
fo	=	fluid outlet
h	=	hydraulic
hsb	=	heat-sink base
ht	=	heater
iw	=	internal wall
j	=	junction
mf	=	mean fluid
o	=	overall
sp	=	spreading
t	=	total
TIM	=	thermal-interface material
w	=	wall

Received 25 July 2008; revision received 6 November 2008; accepted for publication 8 November 2008.

*Energy Conservation and Renewable Energy Group, School of Aerospace, Mechanical and Manufacturing Engineering, Bundoora East Campus, P.O. Box 71; randeep.singh@rmit.edu.au (Corresponding Author).

I. Introduction

WITH the rapid advancement in semiconductor technology, Moore's law [1] prediction that the number of transistors on a microprocessor chip will double about every two years has become a reality. These developments have boosted the processing capabilities and functionalities of the microprocessors, but at the same time, new challenges have been presented in the cooling of these chip sets. Thermal management of the high-density processors in power electronics (including standalone desktops, application servers, and data centers [2,3]) requires continuous research efforts to develop thermal control architectures with cost-effective design and reliable performance. Typically, the waste-heat output by the processing unit in servers can range from 150 to 250 W [4,5] and is expected to rise further in the future with the increase in the number of integrated circuits on a chip set. Such power outputs can result in heat flux as high as 2.5 MW/m^2 from a die footprint of 1 cm^2. Also, as a necessary thermal requirement for the reliable operation and

longevity of a microprocessor, its temperature must be kept below 100°C.

As an appropriate classification, all devices with characteristic dimensions between 1 μm and 1 mm are classified as microdevices. In the past, many researchers have devoted efforts to the development of forced-convection liquid-cooled heat sinks containing microchannels with hydraulic diameters of less than 1 mm. Liquid-cooling can be considered as one of the most viable solutions for thermal control of heat sources with extremely high and concentrated heat fluxes.

Microchannel heat sinks have emerged as one of the effective cooling techniques for high-heat-flux removal in electronic devices. The cold-plate design includes several microchannels and fins arranged in parallel on a metallic substrate with a cover plate for flow management. These microchannels provide extended surface area for heat transfer to the coolant. Because of the extremely small hydrodynamic diameter and high surface-area-to-volume ratio of the microchannels, the heat transfer capacity of the microchannel heat sink is an order of magnitude greater than the simple heat-spreader plate.

Tuckerman and Pease [6] first introduced the concept of microchannels in 1981 and built a water-cooled integral heat sink with microscopic flow channels machined on a silicon wafer. The designed microchannel heat sink was able to dissipate heat flux as high as 790 W/cm^2 with the chip temperature kept below 110°C and successfully demonstrated that extremely-high-power chips can be effectively cooled using microchannel heat transfer. Their results also indicated that the heat transfer coefficient of laminar flow through microchannels might be higher than that of turbulent flow through normally sized channels.

Following the work of Tuckerman and Pease [6], numerous studies such as [7] have been performed in the area of microchannels for heat transfer applications. Peng et al. [8,9] experimentally investigated the flow and heat transfer characteristics of water flowing through rectangular stainless steel microchannels with hydraulic diameters of 133 to 367 μm and channel aspect ratios of 0.33 to 1. In the study, the onset of transition was observed to occur at Reynolds numbers from 200 to 700.

Experiments were conducted by Wang and Peng [10] to study the single-phase forced convection of water and methanol flowing through rectangular microchannels machined on a stainless steel plate. Six kinds of microchannel structures with different widths between 0.2 and 0.8 mm and identical heights of 0.7 mm were used in the investigation. It was observed that a fully developed heat transfer regime is initiated at approximately $Re = 1000$ to 5000, and the transition to turbulent mode is influenced by liquid temperature, velocity, and microchannel size. Transition and laminar heat transfer in microchannels proved to be very complicated when compared with the conventional large-channel-size situation.

Qu et al. [11] investigated the heat transfer characteristics of water flowing through trapezoidal silicon microchannels with hydraulic diameters ranging from 62 to 169 μm. Rahman [12] conducted experimental measurements for pressure drop and convective heat transfer in a microchannel heat sink with water as the coolant. Fabrication of the devices was carried out using standard silicon-100 wafers with a channel width of 1 mm, and the spacing between the channels was 2 mm. Wu and Cheng [13] experimentally investigated 13 different trapezoidal silicon microchannels with hydraulic diameters in the range of 25.1 to 29.1 μm. They found that the Nusselt number increased almost linearly with the Reynolds number.

Microchannel heat sinks have been extensively explored for the chip-cooling applications by different researchers. Zhang et al. [14] reported a study on a single-phase liquid-cooled microchannel heat sink for cooling high-heat-flux electronic packages. The microchannel heat sink was made from aluminum, each channel was 0.21 mm wide and 2 mm high, and deionized water was used as the coolant. Two chip-array packages with different chip footprints, 12×12 mm^2 and 10×10 mm^2, were used for high-heat-flux characterizations. In the tested flow-rate range, the measured junction-to-inlet fluid thermal resistance ranged from 0.44 to 0.32°C/W for the 12 mm chip, whereas for the 10 mm chip, higher thermal resistance ranging from 0.59 to 0.44°C/W was obtained due to larger heat-spreading resistance.

Chang et al. [15] conducted experimental and numerical investigation on the microchannel heat exchanger fabricated directly in the back of silicon chips under uniform heating with a 10×13 mm^2 heater and nonuniform heating with a 400×400 μm hot spot on the chip. Three different microchannel designs with 25, 66, and 100 channels and width, height, and length in the range of 61 to 300 μm, 80 to 295 μm, and 13 to 15 mm, respectively, were fabricated. The lowest thermal resistance of $0.09°C \cdot cm^2/W$ was obtained using a microchannel 61 μm wide and 272 μm deep.

In recent studies, the similarity in the behavior of the microchannels and the convectional channels has been confirmed. However, for the reliable prediction of the flow and heat transfer characteristics inside the microchannel, accurate information on the physical properties and surface morphology of the channels is required. Qu and Mudawar [16] validated and positively confirmed the use of conventional Navier–Stokes equations for microchannels by comparing the experimental and numerical results for pressure drop and heat transfer characteristics of single-phase laminar flow in 231 by 713 μm channels. Lee et al. [17] conducted a systemic investigation of single-phase heat transfer in rectangular microchannels with hydraulic diameters ranging from 318 to 903 μm at flow Reynolds number of 300 to 3500. The heat sink was machined on a copper substrate, and deionized water was used as the working fluid. In the study, numerical predictions were obtained based on a classical continuum approach and were found to be in close agreement with the experimental data. Liu and Garimella [18] reliably predicted the laminar flow characteristics in rectangular microchannels over a hydraulic diameter range of 244 to 974 μm using conventional correlations.

From the literature review, it is evident that the cooling performance of the single-phase liquid-cooling systems can be greatly improved by using microchannel (or microfins) on the fluid side of the cold plate (or cooling section). Different cold-plate materials (including silicon, stainless steel, aluminum, and copper) have been employed for the fabrication of these microchannel heat sinks. From the heat transfer point of view, copper can be considered as the most optimum choice, due to its high thermal conductivity ($\sim$400 $W/m \cdot K$), availability in pure form at reasonable cost, and ease of machinability.

In the category of coolants, water is the most favorable option, with superior heat transfer characteristics, availability in high assay levels at cheaper cost, and nontoxic nature. The present study aims to explore the fluid flow and heat transfer characteristics of the copper-based microchannel heat sink with water as the working fluid for the cooling of high-powered microprocessors. The combination of copper and water is appropriate in heat transfer applications due to their optimal thermal properties and chemical compatibility with each other. Note that there is limited available experimental data on the copper microchannel heat sink with water as the coolant; therefore, the current study will also attempt to provide thermal-fluid characteristics of this combination.

II. Description of the Experimental Prototype

The layout of the microchannel heat sink, as shown in Fig. 1a, includes the bottom plate on which microchannels are fabricated and the top-cover arrangement for flow management. Microchannels were fabricated on a copper block, 54 mm long by 26 mm wide by 5 mm high, by a wire-cutting technique. There were a total of 49 channels in the finned area, 30 mm long by 20 mm wide, and each channel was 0.2 mm wide and 3.5 mm high. The large aspect ratio of 17.5 for the channels was purposely made to enlarge the surface area for heat transfer augmentation. The active heating zone that relates to the microchanneled area in which the heater footprint can be attached was 23.8×23.8 mm^2, as depicted in Fig. 1b.

To avoid deformation of the heating face under attachment pressure from the heat-load simulator, the active zone was approximately 0.5 mm thicker than the rest of the plate. The inlet and outlet plenums were machined in the top-cover portion of the heat

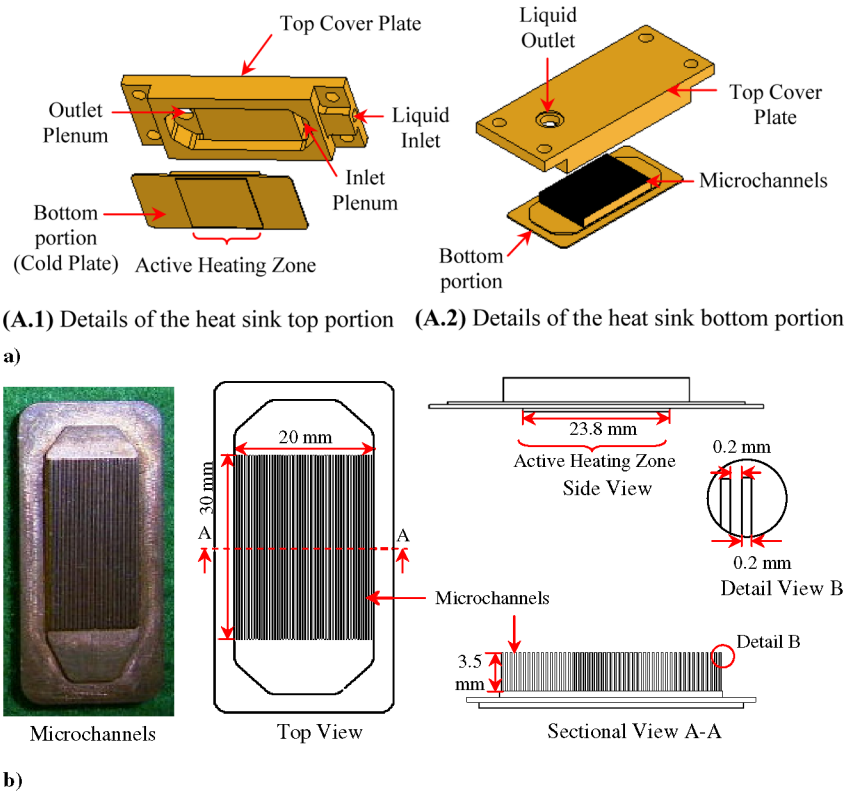

Fig. 1 Detailed description of the microchannel heat-sink assembly: a) exploded view of the microchannel heat-sink assembly showing the top and bottom portions and b) picture and schematics of the microchannels.

sink. These plenums help to achieve efficient coolant distribution through the microchannels. The top cover and the bottom finned plate were attached by brazing to provide proper sealing.

During the assembly of the two halves of the heat sink, proper care should be taken to avoid any gap between the top of the microfins and the inner machined cavity of the top-cover plate. In the case of improper contact, the existing gap will provide a least-resistance flowpath to the fluid, thereby reducing the quantity of the liquid flowing through the microchannels, which will severely hamper the performance of the heat sink. To guarantee proper sealing in the present design, positive clearance was kept between the microfin height and the machined cavity of the top-cover plate.

The coolant enters the heat sink via the inlet tube and collects in the inlet plenum, where it is equally distributed through the microchannels. While flowing through the microchannels, the liquid acquires heat from the large exposed surface of the channel walls (microfins) through convection heat transfer, which results in its temperature rise. The hot liquid collects in the outlet plenums and exits through the outlet tube connected to the top of the cover plate. The liquid flow pattern through the microchannel heat sink is shown in Fig. 2.

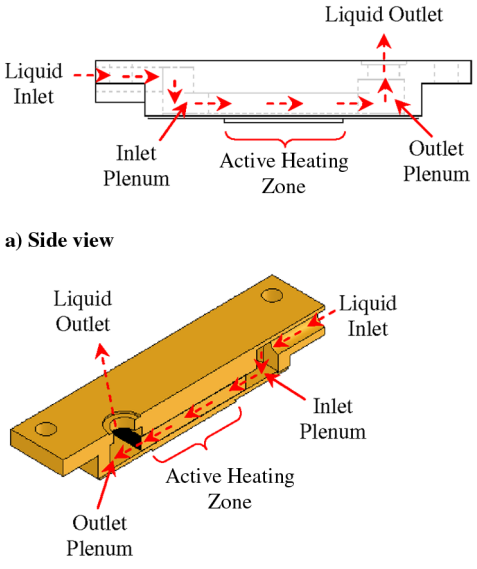

Fig. 2 Internal details and liquid flowpath through the microchannel heat sink.

III. Experimental Setup and Test Procedure

Figure 3 shows the experimental setup that was used to test the thermal performance of the microchannel heat sink. It consists of a microchannel test section, finned heat exchanger, flow tubes, and an electric pump. The heat-load simulator (i.e., heater), in the form of a copper block embedded with two cartridge heaters, was tightly secured to the active zone of the test section with the help of a screw-flange arrangement. To provide better thermal contact between the heater and the heat-sink active zone, thermally conductive grease was used at the interface between the bottom of the heat sink and the top active footprint of the heater. The liquid was pumped through the heat sink with the help of an electric pump, which helped to transfer the heat applied to the active zone of the test section by forced convection of the coolant flowing through the microchannels.

As the present prototype of the microchannel heat sink was designed to handle large heat loads, a collector-type finned heat exchanger with well-developed external and internal surfaces was used for sensible cooling of the liquid leaving the microchannel heat sink. The finned heat exchanger incorporated a bottom header that helped to distribute the hot liquid equally among six tubes passing through the heat exchanger fins. On the other end of the heat exchanger, the top header collected the cold fluid and passed it to the pump for recirculation. The finned heat exchanger was fully made from copper. To avoid corrosion, the heat exchanger fins were nickel-plated. Figure 4 presents the cross-sectional view of the

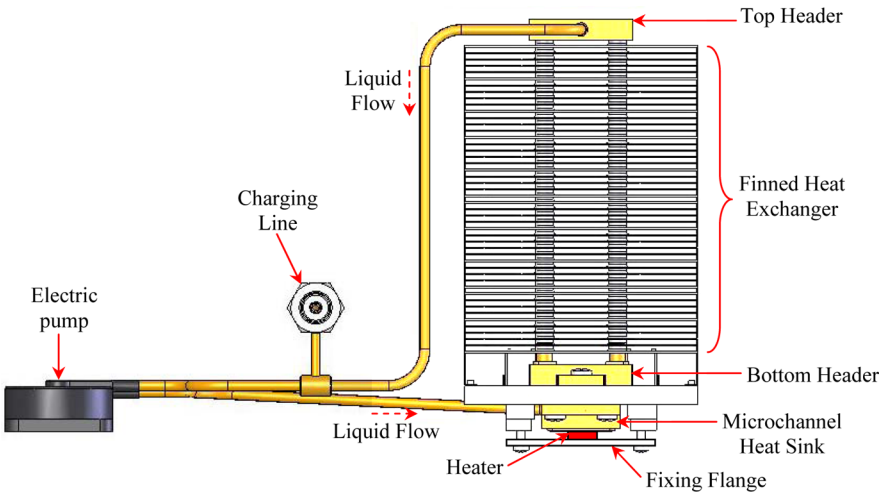

Fig. 3 Experimental setup for microchannel heat sink.

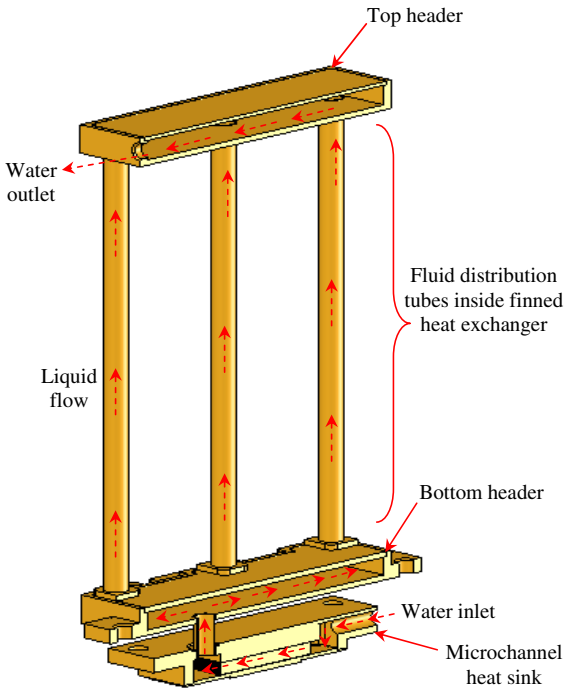

Fig. 4 Cross-sectional view of the microchannel heat sink and distributed finned heat exchanger showing the fluid flow pattern inside the cooling unit (fins are not shown, for visual clarity).

cooling unit, showing the coolant flow through the microchannel heat sink, bottom header, tubes connecting the headers, and top header.

The finned heat exchanger was cooled with the help of forced-air convection by placing it inside a wind tunnel, as shown in Fig. 5. Throughout the test period, the room air temperature was kept constant at 22 ± 2°C. The wind tunnel helped to maintain uniform and well-distributed air passage through the heat exchanger section and to thereby provide stable conditions to perform the experiment. A sufficient airflow rate was maintained through the heat exchanger to dissipate all of the heat input at the microchannel heat sink. The thermal performance of the cooling unit was tested at different coolant flow rates using either open- or closed-loop systems, as presented in Fig. 6. In the open-loop system, as shown in Fig. 6a, the test unit was connected to the constant-temperature water supply from a reservoir, and the liquid flow rate through the microchannel section was controlled by using a control valve at the heat-sink inlet. With this arrangement, high flow rates were achievable, which were useful for testing the maximum heat capacity of the heat sink. During testing, the inlet temperature of the coolant was kept constant at 14 ± 2°C. The mass flow rate of coolant through the microchannels was primarily determined by measuring the mass of liquid flowing through the heat sink over a fixed time interval. Precise measurements for mass were done using a mass balance of sensitivity of 0.01 g.

For the closed-loop system, as shown in Fig. 6b, a centrifugal pump made by SEPA, with a maximum flow rate of 0.43 liters/min at 0 Pa and maximum pressure equivalent to a 60 cm water head at 0 liters/min, was used to circulate liquid through the loop. The pump was rated for 12 V and 0.2 A. Charging of the closed-loop system was done after evacuating the air from the system using a vacuum pump. Distilled water was used as the coolant inside the cooling unit. As the

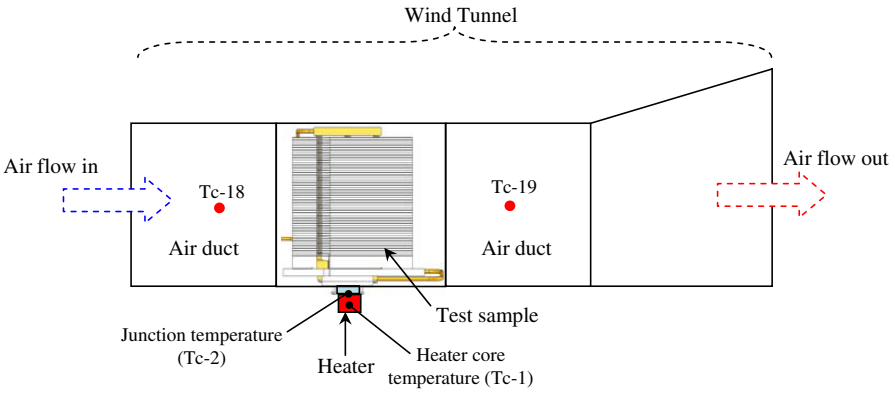

Fig. 5 Testbed for the microchannel heat sink.

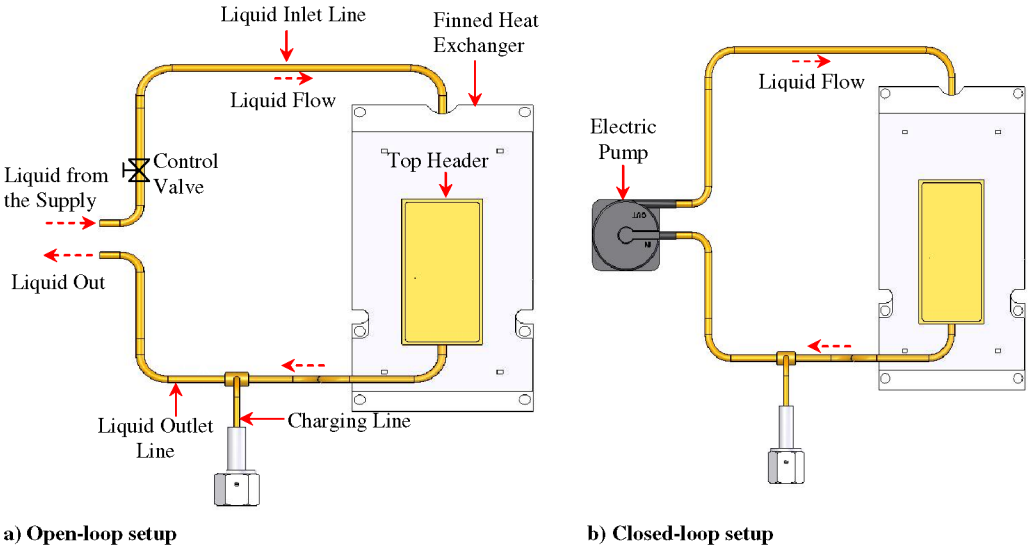

Fig. 6 Experimental setup for microchannel heat sink.

mode of the heat transfer in this case is forced convection using a single phase (i.e., liquid cooling), the cooling unit was fully charged with the working fluid. The thermal characteristics of the microchannel heat sink were studied using 19 T-type thermocouples that were installed at different locations of the cooling unit, as shown in Figs. 7a and 7b. Data from the thermocouples were monitored and recorded every 5 s by using a Keyence data acquisition system connected to a computer.

The temperature at the junction between the heater and the heat-sink cold plate was recorded with the help of a thermocouple (Fig. 5) that was fixed inside the groove machined in the center of the top active heater surface using thermally conductive epoxy. Four thermocouples (Fig. 7a) were mounted on the outer wall of the microchannel heat sink to measure the mean temperature of the cooling section. In addition, seven thermocouples (Fig. 7b) were installed at different locations on the finned-heat-exchanger section to measure its mean wall temperature by an averaging technique.

The outlet temperature of the hot liquid leaving the microchannel was measured by a thermocouple installed at the external surface of the outlet plenum (Tc-7 in Fig. 7a). A thermocouple positioned immediately upstream of the microchannels was used to determine the inlet fluid temperature (Tc-3 in Fig. 7a). The rise in temperature of the cooling air was determined with the help of the two thermocouples at the entrance and exit of the finned heat exchanger, respectively, as shown in Figs. 5 and 7b. A digital wattmeter was used to measure and adjust the input power by changing the input voltage and current. Tests were performed in the power range of 25 to 200 W and coolant-flow-rate range of 1.7 to 15 cm^3/s. The input power and the mass flow rate of coolant were used as the primary controlling parameters for the experiment.

The following procedure was followed to conduct each test. Initially, the fluid circulation through the microchannel was started by opening the control valve (for an open-loop test) or turning on the electric pump (for a closed-loop test). The desired flow rate could be set by adjusting the control valve or changing the input power to the pump. After the flow rate was stabilized, the heater power supply was switched on and the input heat load was set to the fixed value. For steady state, the temperature at different locations on the cooling section had to be kept stable within $\pm 1°C$ limit. After steady state was achieved, readings from all of the thermocouples were recorded using data acquisition system.

IV. Data Reduction and Uncertainty Analysis

For the particular input heat load and mass flow rate (i.e., Reynolds number) of the coolant, fluid flow and forced-convection heat transfer analysis of the microchannel was carried out. In the hydraulic analysis, the total pressure drop incurred by the coolant while flowing through the microchannels was reported. The thermal characteristics of the heat sink were calculated on the basis of the steady-state junction temperature, cold-plate thermal resistance, and convection heat transfer coefficient.

In the present tests, coolant flow rate was kept between 1.7 and 15 cm^3/s, which corresponds to laminar flow through the

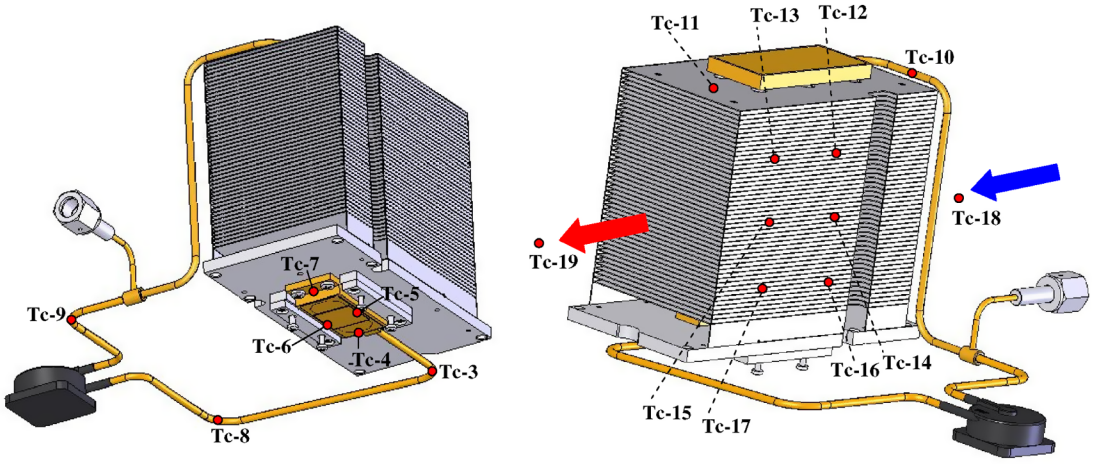

Fig. 7 Test facility for the heat sink showing the location of the thermocouples on the a) microchannel heat sink and b) finned heat exchanger.

microchannels with a Reynolds number of 20 to 150. The pressure drop ΔP due to friction losses in liquid flow through the microchannels is given by the Darcy–Weisbach equation [19] as

$$\Delta P = f\frac{l_{\mathrm{ch}}}{D_h}\frac{\rho U^2}{2} \tag{1}$$

where f is the Darcy friction factor, which can be determined for laminar flow by using the subsequent correlation:

$$f = \frac{64}{Re}, \qquad Re < 2300 \tag{2}$$

Heat losses to ambient from the exposed surfaces of the heat-generating block and cold plate (as approximated by heat balance between the input power by heater and the rise in coolant enthalpy through heat sink) was 6 to 12% of the input power. In the analysis, the thermodynamic properties of the fluid were calculated on the basis of the mean fluid temperature T_{mf} (average of the fluid inlet and outlet temperatures):

$$T_{\mathrm{mf}} = \left(\frac{T_{\mathrm{fo}} + T_{\mathrm{fi}}}{2}\right) \tag{3}$$

The applied heat load $Q_a^{\bullet}$ was determined from the measured input voltage V and current I as follows:

$$Q_a^{\bullet} = VI \tag{4}$$

The convection heat transfer coefficient h_c for the microchannel heat sink is determined from

$$h_c = \frac{Q_a^{\bullet}}{\eta_o A_t (T_{\mathrm{iw}} - T_{\mathrm{mf}})} \tag{5}$$

In Eq. (5), A_t is the total heat transfer area available for convection and is equal to $NA_f + A_b$, where N is the total number of microfins, $A_f = 2l_f d_{\mathrm{ch}}$ is the exposed fin area, and $A_b = (N-1)t_{\mathrm{ch}}l_f$ is the microchannel-base area exposed for convection heat transfer.

The overall efficiency of the microfin array, η_o, is defined as

$$\eta_o = 1 - \frac{NA_f}{A_t}(1 - \eta_f) \tag{6}$$

where η_f is the fin efficiency, which can be found as

$$\eta_f = \frac{\tanh md_{\mathrm{ch}}}{md_{\mathrm{ch}}} \tag{7}$$

and m can be calculated from

$$m = \sqrt{\frac{\bar{h}P_{\mathrm{fc}}}{k_f A_{\mathrm{fc}}}} \tag{8}$$

where $\bar{h} = k_f Nu/D_h$ is the average heat transfer coefficient, as determined from the information on the microchannel aspect ratio $\alpha = d_{\mathrm{ch}}/t_{\mathrm{ch}}$ and Nusselt number Nu for the fully developed laminar flow through rectangular channel at uniform surface temperature [20]; $P_{\mathrm{fc}} = 2(l_f + t_f)$ is the perimeter; and $A_{\mathrm{fc}} = l_f t_f$ area of the microfin cross section.

In Eq. (5), T_{iw} is the internal wall temperature of the microchannel base. As direct measurements of the microchannel wall temperature were not taken, it was determined by extrapolation from the mean temperature of the heat-sink base or cold-plate external surface T_{ew} as follows:

$$T_{\mathrm{iw}} = T_{\mathrm{ew}} - \frac{Q_a^{\bullet} t_{\mathrm{hsb}}}{A_{\mathrm{hsb}} k_{\mathrm{hsb}}} \tag{9}$$

In Eq. (9), T_{ew}, A_{hsb}, and t_{hsb} are the temperature, area, and thickness of the heat-sink base, and k_{hsb} is the thermal conductivity of the base, which is made of copper.

To determine the overall effectiveness of the heat sink, thermal resistance of the cold plate was calculated from

$$R_{\mathrm{cp}} = \frac{(T_j - T_{\mathrm{mf}})}{Q_a^{\bullet}} \tag{10}$$

where T_j is the junction temperature at the interface between the heat-sink base and heat source.

The breakdown analysis of the cold-plate thermal resistance was also done to quantify the thermal resistances of the different components that make up the overall heat-sink resistance. Figure 8 presents the thermal-circuit diagram for the heat flow though the microchannel heat sink with different resistances and the associated temperature-measurement points. These thermal resistances are defined by the following relations:

Heat-spreading thermal resistance:

$$R_{\mathrm{sp}} = \frac{(T_{\mathrm{az}} - T_{\mathrm{iw}})}{Q_a^{\bullet}} \tag{11}$$

Convection thermal resistance:

$$R_c = \frac{(T_{\mathrm{iw}} - T_{\mathrm{mf}})}{Q_a^{\bullet}} \tag{12}$$

In the relations, the cold-plate active zone temperature T_{az}, as represented in Fig. 8, is calculated from Eq. (13) by using information on the junction temperature T_j and contact resistance R_{ct} of the thermal-interface material used at the heater/cold-plate interface:

$$T_{\mathrm{az}} = T_j - Q_a^{\bullet} R_{\mathrm{ct}} \tag{13}$$

where contact thermal resistance is given by

$$R_{\mathrm{ct}} = \frac{t_{\mathrm{TIM}}}{k_{\mathrm{TIM}} A_{\mathrm{ht}}} \tag{14}$$

In the present case, thermally conductive silicon grease was used as the thermal-interface material (TIM). Considering perfectly smooth mating surfaces and assuming a thermal conductivity of 5 $\mathrm{W/m \cdot K}$ and bold-line thickness (or TIM thickness) of 2 mil (1 mil = 0.0254 mm) for the thermal-interface material [21], the contact resistance can be approximated.

In the experiments, thermocouples were calibrated with an accuracy of $\pm 0.1^{\circ}\mathrm{C}$ using a precise constant-temperature bath. For the heat-sink dimensions, the machining tolerance was accurate within ± 50 μm. The wattmeter used to measure the applied heat load to the heat-sink active zone introduces an error of ± 0.1 W. In the determination of heat transfer coefficient from applied heat load $Q_a^{\bullet}$, total heat transfer area A_t and difference of mean cold-plate internal wall to mean fluid temperature ($T_{\mathrm{iw}} - T_{\mathrm{mf}}$), the maximum uncertainty was up to 18.7%. Note that the error in the calculation of h_c was high for low heat loads and high coolant mass flow rates, due to a small temperature difference between the heat transfer surfaces and the coolant. The experimental results revealed a maximum uncertainty of 2.4% for cold-plate thermal resistance.

V. Results and Discussion

A. Pressure Drop

Figure 9 presents the pressure drop through the microchannel heat sink for different flow rates using the open-loop system. It is evident from the graph that the pressure drop showed a linear dependence on the coolant flow rate with a maximum of 3.3 kPa at 15 $\mathrm{cm^3/s}$. The high hydraulic resistance is encountered due to the microscopic structure of the channels and large surface contact area between the coolant and channel walls. On the graph, the pump operating curve is plotted to find the point of operation for the pump when the system was working in closed-loop mode. In this case, the pump was able to provide a coolant flow rate of 5.7 $\mathrm{cm^3/s}$ for a 1.2 kPa pressure drop.

B. Effect of Heater Sizes

In this test, the thermal performance of the designed microchannel heat sink was tested under different heat fluxes using a heat-load

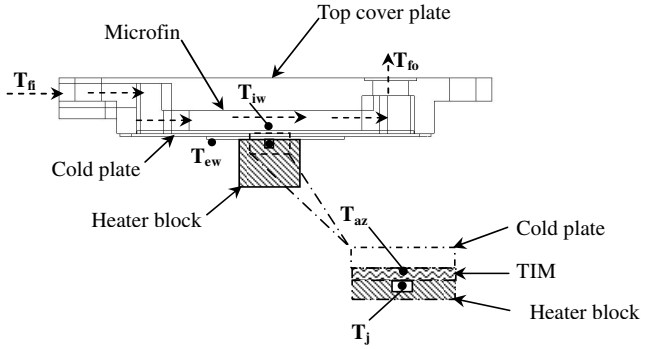

a) Sectional side-view parallel to fluid flow

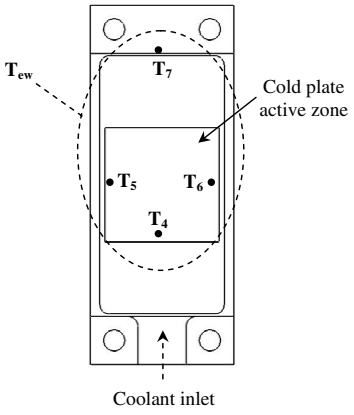

b) Bottom view

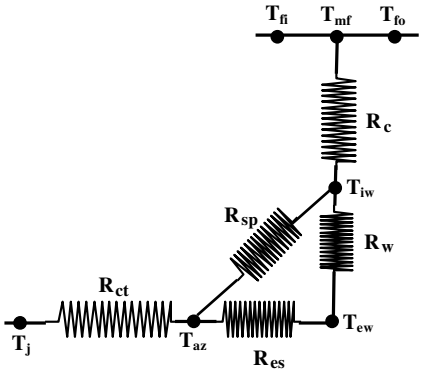

c) Thermal-circuit diagram

Fig. 8 Different components of the cold-plate thermal resistance and the related temperature-measurement points.

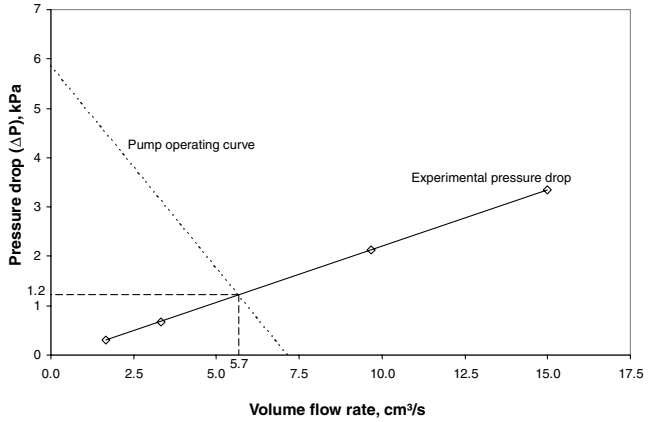

Fig. 9 Pressure drop through the microchannel heat sink versus coolant volume flow rate.

simulator with an active footprint of 11×13 mm^2 and 7×7 mm^2. A heat simulator with an active area of 11×13 mm^2 (i.e., 1.43 cm^2) provides heating to approximately 24% of the active portion (i.e., the region of the heat sink in which the microchannels are present). This results in extremely high heat flux of 140 W/cm^2 at a power dissipation capacity of 200 W from the heat source. For higher-heat-flux characterization of the designed liquid-cooled microchannel heat sink, a heat source with an active footprint as small as 7×7 mm^2 (i.e., 0.49 cm^2) was used to test its performance. Such a heat source supplies concentrated heating to approximately 8.7% of the active face of the cooling section. Here, it contributes to the ultrahigh heat flux of 408 W/cm^2, which can imitate a local hot spot on the high-end chip sets.

In Fig. 10, the heat-load dependence of the temperature at the junction of the heat sink and the 7×7 mm^2 source is plotted and compared with that of the 11×13 mm^2 source for the same cooling conditions at the condenser. This test was carried out using a closed-loop system in which the pump was run at its maximum-rated capacity (12 V, 0.2 A). Because of the smaller size of the 7×7 heater, the steady-state junction temperature achieved in this case was higher than for the 11×13 heater. For example, at a 100 W input load, the junction temperature with the 7×7 heater was approximately 49% higher than that with the 11×13 heater. The junction temperature showed a linear rise with the increase in input heat load. For input power from 25 to 200 W, the junction temperature for the 11×13 heater was between 30 to 64°C, whereas for the 7×7 heat source, the junction temperature was in the high range of 33.6 to 110.4°C.

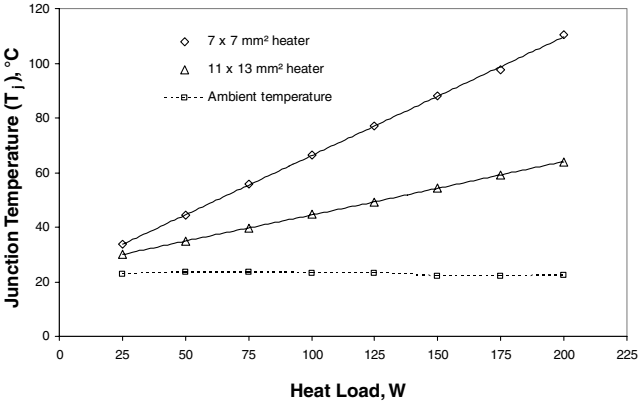

Fig. 10 Heat-load dependence of the junction temperature for the microchannel heat sink with different heater sizes.

Figure 11 presents the results for the cold-plate thermal resistance with respect to the applied heat load. The thermal resistance of the cold plate with the high-flux chip set (i.e., 7×7 mm^2 heater) is 0.33°C/W, compared with 0.11°C/W for the 11×13 mm^2 heater. It is evident from the plotted results that the thermal resistances remains fairly constant (within ± 0.01°C/W) over the entire test range of input heat loads, due to the constant-flow characteristics.

Figure 12 compares the individual components of the cold-plate thermal resistances for the two heaters, as defined in Fig. 8. It is clear from the comparison plot that miniaturization of the die footprint results in the elevation of each resistance component and thus the overall cold-plate resistance. The increase in the contact thermal resistance for the 7×7 source occurs at the expense of a decrease in the heating area A_{ht}, as per Eq. (14). Similarly, for the case of heat spreading from the cold-plate active zone (or heated area on the cold plate) to the inner microchannel base, the condensed size of the heater results in the addition of the metallic resistance offered to the distribution of the heat from the active section of the cooling plate to the microchannel base. Note that the increase rate for the R_{ct} is more than R_{sp}, due to the poor thermal conductivity of the thermal grease material (~ 5 W/m · K), compared with the copper base (~ 400 W/m · K). In the thermal-circuit diagram in Fig. 8c, R_{sp} is divided into two resistance elements: that is, R_{es} and R_w, as per the temperature points of interest on the heat sink.

For convective thermal resistance R_c, the increase for the 7×7 source results even for the same flow character through the microchannels. The 7×7 source provides a higher degree of localized heating ($\sim 8.7\%$) to the microchannel base than the 11×13 source ($\sim 24\%$). This result in large temperature gradients on the microchannel base for the 7×7 source that was heated more in the center than at the sides. As a result, the microchannel walls or microfins are not heated equally along the entire length of the channel, which decreases the sensible heat gain by the coolant from the fins. In contrast, due to the larger active area of the second source (11×13 heater), heat spreading on the microfins and channel walls was better, which improves the convection heat transfer. Note that the net effect of the localized heating in the 7×7 source is the resultant increase in the microchannel-base average temperature, compared with the 11×13 source.

C. Effect of Flow Rate

In the present testing, the thermal characteristics of the microchannel heat sink were studied by varying the flow rate of the coolant from 1.7 to 15 cm^3/s (or 0.1 to 0.9 l/ min). As the electric pump used in the previous testing was capable of providing limited flow rate, the current tests were conducted using an open-loop system, as shown in Fig. 6a. The coolant temperature at the inlet to the heat sink was kept constant at 14 ± 2°C. Testing was done with the high-heat-flux chip set of the 7×7 mm^2 thermal footprint.

The measured junction temperature and cold-plate thermal resistance at different flow rates are shown in Fig. 13 as functions of the applied heat load. As expected, when the flow rate was increased, the junction temperature and the cold-plate thermal resistance dropped. With increasing flow rates, the interface temperature decreased rapidly at first and then at a slower rate. It is further seen that at a given heat load, for high flow rates (above 9.7 cm^3/s), the junction temperature was almost constant and showed little decrease with increase of the flow rate. Note that flow rates beyond 15 cm^3/s were not possible with the current setup, due to the limited fluid-supply pressure available at the inlet to the heat sink.

Similar trends were noted for the cold-plate thermal resistance, as shown in Fig. 13b. The initial increase in the flow rate corresponded to a notable decrease in the thermal resistance, which then became nearly constant for any further increase in the flow rate beyond

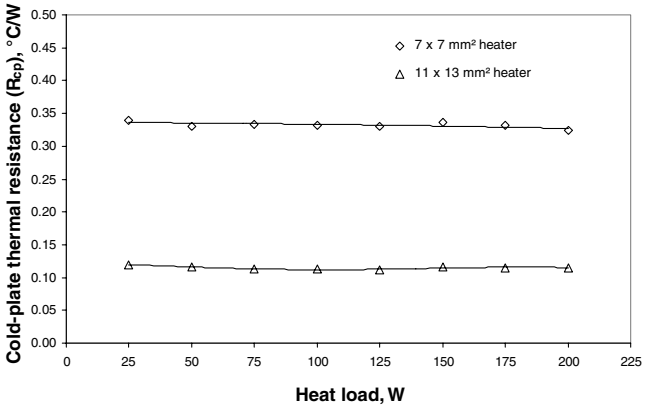

Fig. 11 Cold-plate thermal resistance of the microchannel heat sink with different heater sizes.

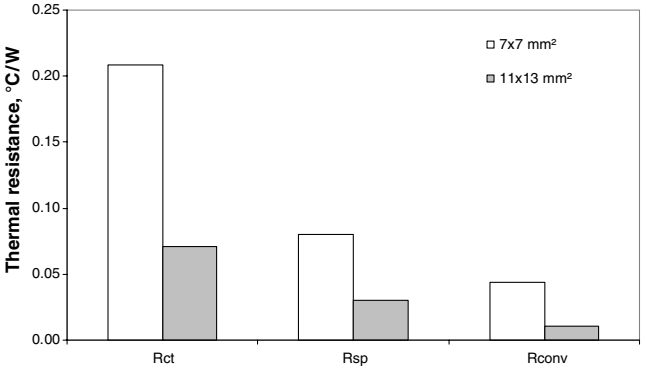

Fig. 12 Relative comparison of different components of the cold-plate thermal resistance for the two heat sources.

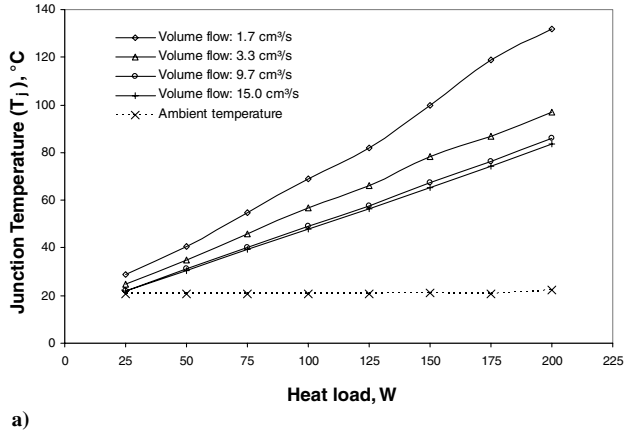

a)

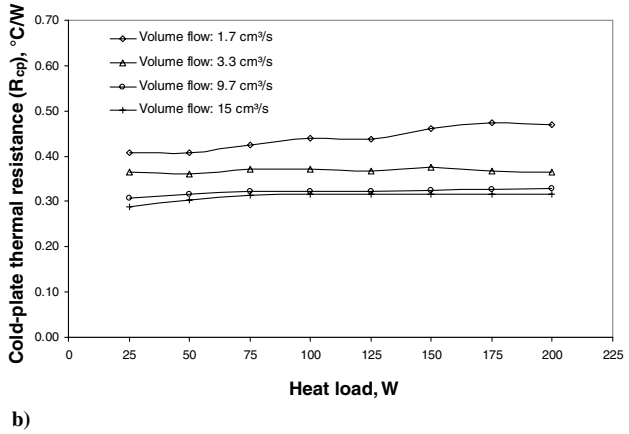

b)

Fig. 13 Variation of the a) junction temperature and b) cold-plate thermal resistance with coolant volume flow rate for the range of applied heat load to the 7×7 mm^2 heater.

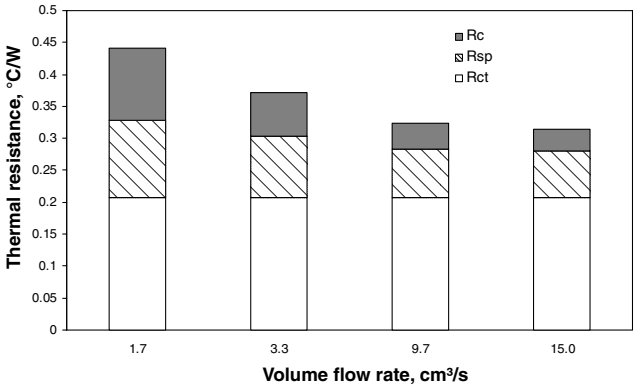

Fig. 14 Relative comparison of different components of the cold-plate thermal resistance at different volume flow rates.

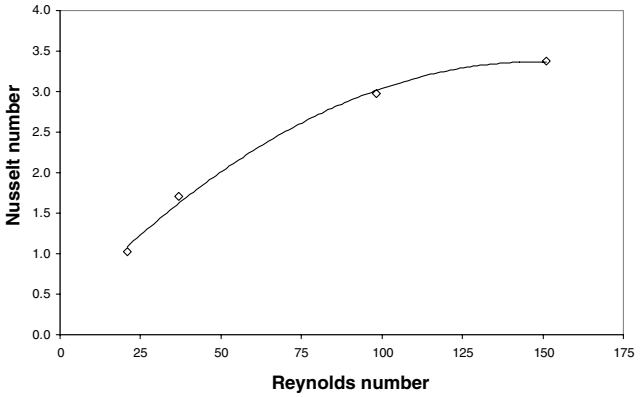

Fig. 16 Relation between Nusselt number versus Reynolds number for the microchannel heat sink.

9.7 cm^3/s at a given input power. For example, at 100 W, the thermal resistance decreased from 0.44 to 0.37°C/W as the flow rate increased from 1.7 to 3.3 cm^3/s, whereas for the same power, the thermal resistance decreased from 0.32 to 0.31°C/W for an increase of flow rate from 9.7 to 15 cm^3/s. This can be explained by considering the total cold-plate thermal resistance through which heat has to pass, starting from the heater top to the coolant.

Figure 14 compares the relative magnitude of each thermal-resistance component at different flow rates and fixed input of 100 W. The total cold-plate thermal resistance in this case is composed of a contact resistance R_{ct} at the heater/cold-plate interface, the conductive resistance R_{sp} to spread heat in the metallic wall of the heat sink, and the convective resistance R_c to transfer heat from the channel inner wall to the coolant. Here, the contact resistance is fixed by the properties of the thermal-interface material and remains constant over the range of coolant flow rates. The spreading resistance is dependent on the physical properties of the cold plate and dimensions of the active heating zone with respect to the total heat acquisition area (microchannel-base area). To some extent, R_{sp} is also affected by the nonlinear dependence of cold-plate temperature on the applied heat load, owing to the three-dimensional heat diffusion from the local heating zone to the bulk of the cold plate. Heat flow always follows the lowest-resistance path. As a result, change in the convection heat transfer inside the microchannel affects the relative magnitude of heat diffusion in the thickness and area plane. At high flow rates, intensification of heat exchange inside microchannels increases the heat flow in the thickness plane, which is evident from the slight decrease in the R_{sp}.

With the initial increase in the flow rate, a considerable decrease in cold-plate thermal resistance due to the enhancement of convective heat transfer from the channel wall to the liquid takes place. However, a point is reached when the maximum possible decrease in the convective resistance is attained at a particular coolant flow rate.

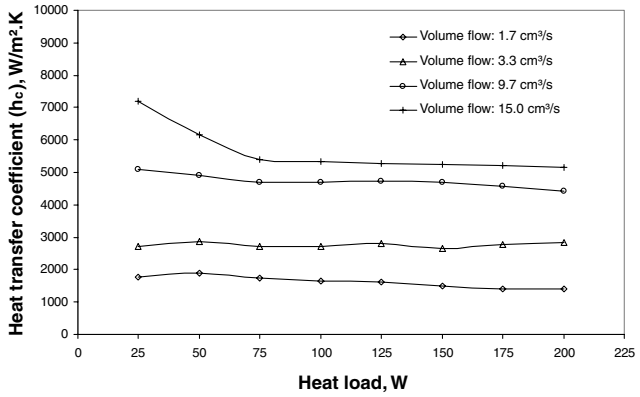

Fig. 15 Heat transfer coefficient versus applied heat load at different volume flow rates for 7 × 7 mm^2 heater.

Beyond this, no further decrease is expected in the resistance, which is now mainly of a conductive nature.

R_{ct} proved to be the main resistance component and contributes to more than 50% of the cold-plate thermal resistance R_{cp}. For a 15 cm^3/s coolant flow rate, R_{ct} was 0.2°C/W (67% of R_{cp}) and R_{sp} and R_c were 0.069°C/W (22% of R_{cp}) and 0.033°C/W (11% of R_{cp}), respectively.

The effect of an increase in the flow rate on the enhancement of the overall heat transfer coefficient is shown in Fig. 15. For an input power of 100 W to the cooling section, as the coolant flow rate was increased from 1.7 to 15 cm^3/s, the convection heat transfer coefficient increased from 1647 to 5334 $W/m^2 \cdot K$. Figure 16 shows the relation between the Nusselt numbers and Reynolds number for the test conditions. A maximum Nusselt number of 3.4 was achieved at the highest experimented Reynolds number of 150.

VI. Conclusions

The results of the investigation can be summarized as follows:

1) A copper-based microchannel heat sink with water as the coolant medium has been developed and characterized for the thermal management of high-end microprocessors in power electronics.

2) Using the designed heat sink, extreme heat fluxes of more than 4.1 MW/m^2 were removed successfully from the heat load while keeping the thermal footprint temperature below 100 ± 5°C.

3) By the use of a miniature electrical pump, minimum values of 0.11 and 0.33°C/W for R_{cp} were achieved with 11×13 mm^2 and 7×7 mm^2 heaters, respectively. Contact resistance at the heater/cold-plate interface proved to be the main component of the overall cold-plate thermal resistance, due to the poor heat conductance of the thermal-interface material.

4) At maximum flow rates of 15 cm^3/s ($Re = 150$) and 100 W input heat, the highest values of 5334 W/m^2.K for convection heat transfer coefficient and 3.4 for Nusselt number were achieved with a 3.3 kPa coolant pressure drop through the microchannel heat sink.

5) With the increase in the coolant flow rate from 1.7 to 15 cm^3/s, the corresponding decrease in the cold-plate thermal resistance from 0.44 to 0.31°C/W was achieved pertaining to the improvement in the convection heat transfer through the microchannels.

6) A copper water-based microchannel heat sink provided a superior heat-augmentation technique to remove high heat fluxes from the source, owing to the high thermal conductivity of the copper and high heat transfer coefficient of the water as a coolant.

References

[1] Moore, G. E., "Cramming More Components onto Integrated Circuits," *Electronics*, Vol. 38, No. 8, Apr. 1965, pp. 114–117; also http://download.intel.com/research/silicon/moorespaper.pdf [retrieved Jan. 2009].

[2] Baer, D. B., "Emerging Cooling Requirements and Systems in Telecommunications Spaces," *Proceedings of the Twenty-Third*

International Telecommunications Energy Conference, Inst. of Electrical and Electronics Engineers, New York, 2001, pp. 95–100.

[3] Schmidt, R. R., Crus, E. E., and Lyengar, M. K., "Challenges of Data Center Thermal Management," *IBM Journal of Research and Development* 49, Nos. 4–5, 2005, 709–723. doi:10.1147/rd.494.0709

[4] Brill, K. G., "2005–2010 Heat Density Trends in Data Processing, Computer Systems, and Telecommunications Equipments: Perspectives, Implications, and the Current Reality in Many Data Centers," Ver. 2.0, Uptime Inst., Santa Fe, NM, 2005, pp. 1–16.

[5] Patel, C. D., Sharma, R., Bash, C. E., and Beitelmal, A., "Thermal Consideration in Cooling Large Scale High Compute Density Data Centers," *Proceedings of the 80th Intersociety Conference on Thermal and Thermomechanical Phenomena in Electronic Systems*, Inst. of Electrical and Electronics Engineers, New York, 2002, pp. 767–776.

[6] Tuckerman, D. B., and Pease, R. F. W., "High Performance Heat Sinking for VLSI," *IEEE Electron Device Letters*, Vol. 2, No. 5, 1981, pp. 126–129. doi:10.1109/EDL.1981.25367

[7] Morini, G. L., "Single-Phase Convective Heat Transfer in Microchannels: A Review of Experimental Results," *International Journal of Thermal Sciences*, Vol. 43, 2004, pp. 631–651. doi:10.1016/j.ijthermalsci.2004.01.003

[8] Peng, X. F., Peterson, G. P., and Wang, B. X., "Frictional Flow Characteristics of Water Flowing Through Microchannels," *Experimental Heat Transfer*, Vol. 7, No. 4, 1994, pp. 249–264 doi:10.1016/0140-6701(95)97177-L.

[9] Peng, X. F., Peterson, G. P., and Wang, B. X., "Heat Transfer Characteristics of Water Flowing Through Microchannels," *Experimental Heat Transfer*, Vol. 7, No. 4, 1994, pp. 265–283. doi:10.1016/0140-6701(95)97179-N

[10] Wang, B. X., and Peng, X. F., "Experimental Investigation on Liquid Forced Convection Heat Transfer Through Microchannels," *International Journal of Heat and Mass Transfer*, Vol. 37, Supplement 1, 1994, pp. 73–82. doi:10.1016/0017-9310(94)90011-6

[11] Qu, W., Mala, G. M., and Li, D., "Heat Transfer for Water Flow in Trapezoidal Silicon Microchannels," *International Journal of Heat and Mass Transfer*, Vol. 43, No. 21, 2000, pp. 3925–3936. doi:10.1016/S0017-9310(00)00045-4

[12] Rahman, M. M., "Measurements of Heat Transfer in Microchannel Heat Sinks," *International Communications in Heat and Mass Transfer*, Vol. 27, No. 4, 2000, pp. 495–506. doi:10.1016/S0735-1933(00)00132-9

[13] Wu, H. Y., and Cheng, P., "An Experimental Study of Convective Heat Transfer in Silicon Microchannels with Different Surface Conditions," *International Journal of Heat and Mass Transfer*, Vol. 46, No. 14, 2003, pp. 2547–2556. doi:10.1016/S0017-9310(03)00035-8

[14] Zhang, H. Y., Pinjala, D., Wong, T. N., Toh, K. C., and Joshi, Y. K., "Single-Phase Liquid Cooled Microchannel Heat Sink for Electronic Packages," *Applied Thermal Engineering*, Vol. 25, No. 10, 2005, pp. 1472–1487. doi:10.1016/j.applthermaleng.2004.09.014

[15] Chang, J. Y., Prasher, R., Chau, D., Myers, A., Dirner, J., Prstic, S., and He, D., "Convective Performance of Package Based Single Phase Microchannel Heat Exchanger," ASME IPACK2005, San Francisco, American Society of Mechanical Engineers Paper 73126, 2005.

[16] Qu, W., and Mudawar, I., "Experimental and Numerical Study of Pressure Drop and Heat Transfer in a Single-Phase Microchannel Heat Sink," *International Journal of Heat and Mass Transfer*, Vol. 45, No. 12, 2002, pp. 2549–2565. doi:10.1016/S0017-9310(01)00337-4

[17] Lee, P. S., Garimella, S. V., and Liu, D., "Investigation of Heat Transfer in Rectangular Microchannels," *International Journal of Heat and Mass Transfer*, Vol. 48, No. 9, 2005, pp. 1688–1704. doi:10.1016/j.ijheatmasstransfer.2004.11.019

[18] Liu, D., and Garimella, S. V., "Investigation of Liquid Flow in Microchannels," *Journal of Thermophysics and Heat Transfer*, Vol. 18, No. 1, 2004, pp. 65–72. doi:10.2514/1.9124

[19] Cengel, Y. A., and Turner, R. H., *Fundamentals of Thermal-Fluid Sciences*, McGraw–Hill, New York, 2001, Chap 18 and 19.

[20] Incropera, F. P., and DeWitt, D. P., *Fundamentals of Heat and Mass Transfer*, Wiley, Hoboken, NJ, 2001.

[21] Samson, E. C., Machiroutu, S. V., Chang, J. Y., Santos, I., Hermerding, J., Dani, A., Prasher, R., and Song, D. W., "Interface Material Selection and a Thermal Management Technique in Second-Generation Platforms Built on Intel® Centrino™ Mobile Technology," *Intel Technology Journal*, Vol. 9, No. 1, 2005, pp. 75–86; also http://download.intel.com/technology/itj/2005/volume09issue01/art06_interface_materials/vol09_art06.pdf [retrieved Jan. 2009].